Forecast sensitivity to observations (FSO) as a diagnostic tool: monitoring the impact of observations on the short range forecast

Carla Cardinali and Fernando Prates

European Centre for Medium-Range Weather Forecasts
Reading, UK
carla.cardinali@ecmwf.int and fernando.prates@ecmwf.int

Abstract

This paper describes the use of forecast sensitivity to observations as a diagnostic tool to monitor the observation impact on the quality of the short range forecasts (typically 24 hour). The forecast error is provided by a control experiment (using all observations available) which has been run among two series of observing system experiments performed at ECMWF. The observation data impact obtained with the forecast sensitivity is then compared with the observation data impact as classically measured in the context of observing system experiments. Overall, the assimilated observations decrease the forecast error. However, locally some poor performances are detected that are related either to the data quality or biases in the model.

1. Introduction

Over the last decade, data assimilation schemes have evolved towards very sophisticated systems, such as the four-dimensional variational system (4D-Var) (Rabier *et al.* 2000) that operates at the European Centre for Medium-Range Weather Forecasts (ECMWF). The scheme handles a large variety of both space and surface-based meteorological observations. It combines the observations with prior (or background) information on the atmospheric state and uses a comprehensive (linearized) forecast model to ensure that the observations are given a dynamically realistic, as well as statistically likely response in the analysis. Effective performance monitoring of such a complex system, with an order of 10^7 degrees of freedom and more than 10^6 observations per 12-hour assimilation cycle, has become an absolute necessity.

The assessment of each observation contribution to the analysis is among the most challenging diagnostics in data assimilation and numerical weather prediction. Methods have been derived to measure the observational influence in data assimilation schemes (Purser and Hung 1993, Cardinali *et al*. 2004, Fisher 2003, and Chapnick *et al*. 2004). These techniques show how the influence is assigned during the assimilation procedure, which partition is given to the observation and which is given to the background or pseudo-observation. They therefore provide a indication of the robustness of the fit between model and observations and allow some tuning of the weights assigned in the assimilation system.

Recently, adjoint-based observation sensitivity techniques have been used (Baker and Daley 2000, Langland and Baker 2004, Cardinali and Buizza, 2004, Morneau *et al*., 2006, Xu and Langlang, 2006, Zhu and Gelaro 2008) to measure the observation contribution to the forecast, where the observation impact is evaluated with respect to a scalar function representing the short-range forecast error. In general, the adjoint methodology can be used to estimate the sensitivity measure with respect to any parameter of importance of the assimilation system. Very recently, Daescu (2008) derived a sensitivity equation of an unconstrained variational data assimilation system from the first order necessary condition with respect to the main input parameters: observation, background and their error covariance matrices. The paper provides the theoretical

framework for further diagnostic tool development not only to evaluate the observation impact on the forecast but also the impact of the other analysis parameters. Sensitivity to background covariance matrix can help in evaluating the correct specification of the background weight and their correlation. Limitations and weaknesses of the covariance matrices are well known, several assumptions and simplifications are made to derive them. Desroziers and Ivanov (2001) and Chapnik et al. (2006) discussed the importance of diagnosing and tuning the error variances in a data assimilation scheme.

Over the past years, Observing System Experiments (OSEs) have been the traditional tool for estimating data impact in a forecasting system (Bouttier and Kelly, 2001 English *et al*., 2004 and Lord *et al*., 2004, Kelly and Thépaut, 2007). Usually, OSEs are performed by removing subsets of observation from the assimilation system and the forecasts are compared against a *control* experiment that includes all observations.

The value of observations in the forecast is assessed by comparing forecast skill obtained by different statistical measures and several independent experiments need to be performed for quite long periods (a few months) to ensure statistical significance to the results. The assessment of the value of a given observation type can become quite expensive if a full investigation of the different components of the GOS (Global Observing System) is performed.

Clearly, there are some basic differences between the adjoint-based observation technique and the OSE technique:

The adjoint-based observation sensitivity technique measures the impact of observations when the entire observation dataset is present in the assimilation system, while the observing system is, in the OSE context, modified. In fact, each OSE experiment differs from the others in terms of assimilated observations.

The adjoint-based observation sensitivity technique measures the response of a single forecast metric to all perturbations of the observing system, while the OSE measures the effect of a single perturbation on all forecast metrics.

The adjoint-based technique is restricted by the tangent linear assumption, valid up to 3 days. Furthermore, a simplified adjoint model is usually used to carry the forecast error information backwards, which limits further the validity of the linear assumption, and therefore restricts the use of the diagnostic to a typical forecast range of 24-48 hours. One implication to use a simplified adjoint model is that the analysis uncertainties obtained throughout the adjoint integration can be incorrect if the propagating back signal is weak (Isakseen et al., 2005). The OSE on the other hand can measure data impact on long-range forecast.

The adjoint-based observation sensitivity technique measures the impact of all observations assimilated at a single analysis time while the OSE includes effect of observations assimilated at previous time since they compare modified Kalman gain matrices.

The aim of this paper is twofold: illustrate the type of investigation and diagnostics that can be carried out with the adjoint-based observation sensitivity in an operational context, and provide the overall observation performance in the system. To this respect the adjoint tool is based on the forecast error of the *control* experiment of those OSEs that have recently been performed at ECMWF (Kelly and Thépaut 2007) and on the forecast error of the last implemented operational model

In this paper, the potential of estimating forecast sensitivity to observations as a diagnostic tool to investigate the sources of short-range forecast errors is shown and qualitatively contrasted with an Observing System Experiment In section 2, the theoretical background of the forecast sensitivity (observation and background), the numerical solution and the calculation of the forecast error contribution from observations are shown.

Also, the OSEs used in the investigation are summarized. Results are illustrated in section 3. Conclusions are given in section 4.

2. Observation Impact on the Forecast

2.1. Linear analysis equation

Data assimilation systems for numerical weather prediction (NWP) provide estimates of the atmospheric state $\mathbf{x}$ by combining meteorological observations $\mathbf{y}$ with prior (or background) information $\mathbf{x}_b$. A simple Bayesian normal model provides the solution as the posterior expectation for $\mathbf{x}$, given $\mathbf{y}$ and $\mathbf{x}_b$. The same solution can be achieved from a classical *frequentist* approach, based on a statistical linear analysis scheme providing the Best Linear Unbiased Estimate (Talagrand 1997) of $\mathbf{x}$, given $\mathbf{y}$ and $\mathbf{x}_b$. The optimal general least square solution to the analysis problem (see Lorenc 1986) can be written

$$\mathbf{x}_a = \mathbf{K}\mathbf{y} + (\mathbf{I}_n - \mathbf{K}\mathbf{H})\mathbf{x}_b \tag{2.1}$$

The vector $\mathbf{x}_a$ is called the 'analysis'. The gain matrix $\mathbf{K}$ (of dimension $n \times p$ with n being the state vector and p the observation vector dimensions) takes into account the respective accuracies of the background vector $\mathbf{x}_b$ and the observation vector $\mathbf{y}$ as defined by the $(n \times n)$-dimensioned covariance matrix $\mathbf{B}$ and the $(p \times p)$-dimensioned covariance matrix $\mathbf{R}$, with

$$\mathbf{K} = (\mathbf{B}^{-1} + \mathbf{H}^T\mathbf{R}^{-1}\mathbf{H})^{-1}\mathbf{H}^T\mathbf{R}^{-1} \tag{2.2}$$

Here, $\mathbf{H}$ is a $(p \times n)$-dimensioned matrix interpolating the background fields to the observation locations, and transforming the model variables to observed quantities (e.g. radiative transfer calculations transforming the model's temperature, humidity and ozone into brightness temperatures as observed by several satellite instruments). In the 4D-Var context, $\mathbf{H}$ also includes the propagation in time of the atmospheric state vector to the observation times using a forecast model. From (2.1) the sensitivity of the analysis system with respect to the observations and the background can be derived from:

$$\begin{aligned} \frac{\partial \mathbf{x}_a}{\partial \mathbf{y}} &= \mathbf{K}^T \\ \frac{\partial \mathbf{x}_a}{\partial \mathbf{x}_b} &= \mathbf{I} - \mathbf{H}^T\mathbf{K}^T \end{aligned} \tag{2.3}$$

The analysis sensitivity with respect to the observation is a similar measure as the observation influence derived by Cardinali *et al*. (2004). The only difference to the 'Influence matrix' is the space in which the solution is found. Here, the analysis sensitivity is found in the model space instead of the observation space.

2.2. Sensitivity gradient

Let consider two forecasts of length f starting from $\mathbf{x}_a$ and length g starting from $\mathbf{x}_b$, $\mathbf{x}_b$ being the background field used in the $\mathbf{x}_a$ analysis. Both forecasts verify at time t. Following Langland and Baker (2004) and Errico (2007) the third order sensitivity gradient is defined as

$$\frac{\partial J}{\partial \mathbf{x}_a} = \frac{\partial J_f}{\partial x_a} + \frac{\partial J_g}{\partial x_b} \tag{2.4}$$

Where $J_f = \left\langle (\mathbf{x}_f - \mathbf{x}_t), \mathbf{C}(\mathbf{x}_f - \mathbf{x}_t) \right\rangle / 2$ and $J_g = \left\langle (\mathbf{x}_g - \mathbf{x}_t), \mathbf{C}(\mathbf{x}_g - \mathbf{x}_t) \right\rangle / 2$ are a quadratic measure of the two forecast errors ($\mathbf{x}_t$ the verifying analysis, taken here as the truth), and $\mathbf{C}$ is a matrix of dry energy norm weighting coefficients. It is clear that from (2.4) the adjoint model maps the sensitivity (with respect to the forecast) of J_f into $\partial J_f / \partial \mathbf{x}_a$ along the trajectory *f* and the sensitivity of J_g into $\partial J_g / \partial \mathbf{x}_a$ along the trajectory *g* (see Rabier *et al*. 1996, Gelaro *et al*., 1998 for the first order sensitivity gradient definition and computation).

2.3. Sensitivity equation

Baker and Daley (2000) derived the forecast sensitivity equation with respect to the observations in the context of variational data assimilation. Let us consider a scalar *J*-function of the forecast error. Then, the sensitivity of J with respect to the observations can be written using a simple derivative chain as:

$$\frac{\partial J}{\partial \mathbf{y}} = \frac{\partial J}{\partial \mathbf{x}_a} \frac{\partial \mathbf{x}_a}{\partial \mathbf{y}} \tag{2.5}$$

where $\partial J / \partial \mathbf{x}_a$ is the sensitivity of the forecast error to the initial condition described in (b) . By using (2.2) and (2.3) the forecast sensitivity to the observations becomes:

$$\frac{\partial J}{\partial \mathbf{y}} = \mathbf{K}^T \frac{\partial J}{\partial \mathbf{x}_a} = \mathbf{R}^{-1}\mathbf{H}(\mathbf{B}^{-1} + \mathbf{H}^T\mathbf{R}^{-1}\mathbf{H})^{-1} \frac{\partial J}{\partial \mathbf{x}_a} \tag{2.6}$$

where $(\mathbf{B}^{-1} + \mathbf{H}^T\mathbf{R}^{-1}\mathbf{H})^{-1}$ is the analysis error covariance matrix **A**.

2.4. Numerical solution

In an optimal variational analysis scheme, the analysis error covariance matrix **A** is approximately the inverse of the matrix of second derivatives (the Hessian) of the analysis cost function J_a (Rabier *et al*. 2000), i.e. $\mathbf{A}=(\mathbf{J_a''})^{-1}$ (Rabier and Courtier 1992). Given the large dimension of the matrices involved, $\mathbf{J_a''}$ and its inverse cannot be computed explicitly. The minimization is performed in terms of a transformed variable χ, $\chi=\mathbf{L}^{-1}(\mathbf{x}-\mathbf{x}_b)$, with **L** chosen such that $\mathbf{B} = \mathbf{L}\mathbf{L}^T$. The transformation **L** thus reduces the covariance of the prior to the identity matrix. In variational data assimilation, **L** is referred to as the change-of-variable operator (Courtier *et al.* 1998). Let apply the change-of-variable in the analysis cost function and write:

$$\begin{aligned} J_a(\mathbf{x}) &= \frac{1}{2}(\mathbf{x}-\mathbf{x}_b)^T\mathbf{B}^{-1}(\mathbf{x}-\mathbf{x}_b) + \frac{1}{2}(\mathbf{H}\mathbf{x}-\mathbf{y})^T\mathbf{R}^{-1}(\mathbf{H}\mathbf{x}-\mathbf{y}) \\ &= \frac{1}{2}\chi^T\chi + \frac{1}{2}(\mathbf{H}\mathbf{L}\chi-\mathbf{y})^T\mathbf{R}^{-1}(\mathbf{H}\mathbf{L}\chi-\mathbf{y}) = J_a(\chi) \end{aligned} \tag{2.7}$$

The Hessian becomes:

$$J_a''(\chi) = \mathbf{I} + \mathbf{L}^T\mathbf{H}^T\mathbf{R}^{-1}\mathbf{H}\mathbf{L} \tag{2.8}$$

By applying the change-of-variable in (2.7) and by using (2.8), the forecast sensitivity to the observations is expressed as:

$$\frac{\partial J}{\partial \mathbf{y}} = \mathbf{R}^{-1}\mathbf{H}\mathbf{L}(\mathbf{I} + \mathbf{L}^T\mathbf{H}^T\mathbf{R}^{-1}\mathbf{H}\mathbf{L})^{-1}\mathbf{L}^T \frac{\partial J}{\partial \mathbf{x}_a} \tag{2.9}$$

Using the conjugate gradient algorithm, first the following equation for $\partial J/\partial \mathbf{y} = \mathbf{R}^{-1}\mathbf{H}\mathbf{z}$ is solved:

$$(\mathbf{I} + \mathbf{L}^T\mathbf{H}^T\mathbf{R}^{-1}\mathbf{H}\mathbf{L})\mathbf{z} = \mathbf{L}\mathbf{z}_a$$
$$\mathbf{z}_a = \frac{\partial J}{\partial \mathbf{x}_a} \qquad 2.10$$

The solution **z** lies in the Krylov-subspace generated by the vector $\mathbf{L}^T\mathbf{z}_a$ and the matrix ($\mathbf{I}+\mathbf{L}^T\mathbf{H}^T\mathbf{R}^{-1}\mathbf{H}\mathbf{L}$). The Krylov-subspace dimension is the degree of the minimal polynomial of ($\mathbf{I}+\mathbf{L}^T\mathbf{H}^T\mathbf{R}^{-1}\mathbf{H}\mathbf{L}$). Therefore if the degree is low, the Krylov-method searches the solution on a small dimensioned space. The method is very efficient in an iterative solution of a linear system with large and sparse matrices (Van der Vorst 2003).

The forecast sensitivity to observations is then given by interpolating **z** (using the **H** operator) in the observation space and by normalizing with respect to the observation error covariance matrix **R**.

2.5. First order sensitivity gradient

Let now compare the first order sensitivity gradient with the third order one. On this subject, let $J_1(\mathbf{e}) = \|\mathbf{e}, \mathbf{C}\mathbf{e}\|$ express the variation in the forecast error due to the assimilation of observations, that is $J(\mathbf{e}_a) - J(\mathbf{e}_b)$ where the $\mathbf{e}_a$ and $\mathbf{e}_b$ are the analysis and the background error. Following Langland and Baker, the second (or third) order Taylor series decomposition (see also Errico 2007) is used to map such variation

$$J(\mathbf{e}_b) - J(\mathbf{e}_a) = (\mathbf{e}_b - \mathbf{e}_a)^T J'_{e_a} + \frac{1}{2}(\mathbf{e}_b - \mathbf{e}_a)^T J''_{e_a}(\mathbf{e}_b - \mathbf{e}_a) \qquad (2.11)$$

Because the error cost function is quadratic, (2.11) reduces to

$$J(\mathbf{e}_b) - J(\mathbf{e}_a) = 2(\mathbf{e}_b - \mathbf{e}_a)^T \mathbf{e}_a + (\mathbf{e}_b - \mathbf{e}_a)^T(\mathbf{e}_b - \mathbf{e}_a) \qquad (2.12)$$

that at the first order is

$$J(\mathbf{e}_b) - J(\mathbf{e}_a) = -2\mathbf{d}^T\mathbf{K}^T\mathbf{e}_a \qquad (2.13)$$

In an optimal assimilation system, the right hand side of the equation is on average zero (Talagrand, 2002) since statistically, the innovation vector, $\mathbf{d}=\mathbf{y}-\mathbf{H}\mathbf{x}_b$, and the analysis error are orthogonal. The results obtained by using the first order sensitivity gradient, only provides the measure of the sub-optimality of the analysis system. Therefore, the second order term appears necessary to be included in the FSO calculation.

All the experiments performed are using a third order sensitivity gradient as described in 2.2.

2.6. Observation impact measure

Once the forecast sensitivity is computed, the variation δJ of the forecast error expressed by J can be found by rearranging (2.1) and by using the adjoint property for the linear operator:

$$\delta J = \left\langle \frac{\partial J}{\partial \mathbf{x}_a}, \delta\mathbf{x}_a \right\rangle = \left\langle \frac{\partial J}{\partial \mathbf{x}_a}, \mathbf{K}(\mathbf{y} - \mathbf{H}\mathbf{x}_b) \right\rangle = \left\langle \mathbf{K}^T \frac{\partial J}{\partial \mathbf{x}_a}, \mathbf{y} - \mathbf{H}\mathbf{x}_b \right\rangle = \left\langle \mathbf{K}^T \frac{\partial J}{\partial \mathbf{x}_a}, \delta\mathbf{y} \right\rangle = \left\langle \frac{\partial J}{\partial \mathbf{y}}, \delta\mathbf{y} \right\rangle \qquad 2.11$$

where $\delta \mathbf{x}_a = \mathbf{x}_a - \mathbf{x}_b$ are the analysis increments and $\delta \mathbf{y} = \mathbf{y} - \mathbf{H}\mathbf{x}_b$ is the innovation vector. This is the first time that δJ has been computed for a 12 hour 4D-Var system; the sensitivity gradient $\partial J / \partial \mathbf{x}_a$ is valid at the starting time of the 4D-Var window (typically 09 and 21 UTC for the 12h 4D-Var set-up used at ECMWF). As for **K**, its adjoint $\mathbf{K}^{\mathrm{T}}$ incorporates the temporal dimension, and the δ**y** innovations are distributed over the 12-hour window. The variation of the forecast error due to a specific measurement can be summed up over time and space in different subsets to compute the average contribution of different component of the observing system to the forecast error. For example, the contribution of all AMSU-A satellite instruments, *s*, and channels, *i*, over time T will be:

$$\delta J_{AMSU-A} = \sum_{\substack{s \in S \\ t \in T}} \sum_{i \in channel} \delta J^{s}_{it}$$

The forecast error contribution can be gathered over different subsets that can represent a specific observation type, a specific vertical or horizontal domain, or a particular meteorological variable.

2.7. Observation system experiment

A traditional way of estimating data impact in a forecasting system is to perform OSEs such as those illustrated by Bouttier and Kelly (2001) or Kelly and Thépaut (2007) (for other weather centres see also English *et al*. 2004 and Lord *et al*. 2004). OSEs can be performed in two ways: in one way, the performance of a baseline (*reference*) experiment which uses a minimum amount of observation types is compared with experiments that add at least one more observation type (Kelly and Thépaut, 2007). The other way consists in removing one particular or various datasets from the full system over a long assimilation period and to then compare the performance with respect to the *control* experiment, which assimilates the fully available observations from the GOS. In either case, it has to be reminded that removing observations from the assimilation system will generate a different Kalman gain matrix.

The assessment of the observation value with respect the forecast skill through OSEs is performed by e.g. comparing the root mean square forecast error, anomaly correlation, etc. obtained with and without the subset of interest. This usually involves several independent experiments over a few months. Therefore, OSEs can be quite costly if a comprehensive investigation of the various contributions of the elements of the GOS needs to be performed. In Table 1 and Table 2, the observations assimilated in the *control* experiment and the list of the OSEs used in the investigation, are summarized. Forecasts have been computed for each OSEs from the 00 UTC analyses only, in order to save computing time.

Table 1: Operational data set in the OSE control experiment for summer 2006 and winter 2007 (Kelly and Thépaut, 2007). T, H, RH, p, u and v stand for temperature, humidity, relative humidity, pressure and u and v wind components.

Type of Data	Description
OZONE	Satellite ozone retrieval
GOES	Geostationary satellite infrared sounder radiances
METEOSAT	Geostationary satellite infrared sounder radiances
AMSU-B	Satellite microwave sounder radiances related to H
SSMI-TCWV	Satellite microwave imager radiances related to clouds and precipitation
SSMI	Satellite microwave imager radiances related to H and surface wind speed
AIRS	Satellite infrared sounder radiances related to H and T
AMSU-A	Satellite microwave sounder radiances related to T
HIRS	Satellite infrared radiances
ERS-QuikSCAT	Satellite microwave scatterometer
AMVs	Atmospheric Motion Vectors derived from satellite cloud imagery
GPS-RO	Satellite GPS radio occultation
PILOT	Sondes and American, European and Japanese Wind profiler (u,v)
TEMP	Radiosondes from land and ship measuring ps, T, RH , u and v
AIREP	Aircraft measurements of T, u and v
DRIBU	Drifting buoy measuring ps, T, RH, u and v
SYNOP	Surface Observations from land and ship stations: measuring ps, RH , u and v

Table 2: List of OSEs.

Name	Observations assimilated
Reference	Conventional, AMSU-A from NOAA-16.
AMV	Reference + AMVs

3. Results

The forecast sensitivity to the observation (FSO) has been computed for two seasons, a winter and a summer period, based on the forecast error calculated for the *control* experiment of the OSEs performed by Kelly and Thépaut (2007). The FSO calculation [(2.9) and (2.10)] has been carried out on 60 model levels and with a horizontal truncation of T159 to match with the OSE final inner loop resolution and also based on both 00 and 12 UTC forecast error (only the 00 impact is shown). As for the OSE, the observation departures were computed at T511 (model trajectory resolution, Rabier *et al*. 2000). All the experiments were performed using the third order sensitivity gradient defined in section 2(b). Sensitivity gradients were computed at T159 analysis resolution.

The sensitivity to the humidity initial condition is obtained as a secondary effect due to the adjoint of the linearized moist physical processes used in the sensitivity gradient calculation (Lopez and Moreau 2005, Tompkins and Janisková 2004, Janisková *et al*. 2002) which accounts for the dependency of the forecast error at the verification time due to the humidity errors in the initial conditions. The energy norm diagnostic function was computed from the OSE *control* (using all available observations) experiment forecast error.

In the results presented here, the potential of the FSO diagnostic tool on the contribution of the observing system to the short-range forecast error is investigated and contrasted with that from the OSE tool. Due to the fact that the OSEs medium-range forecast is computed only from the 00 UTC analyses, the FSO diagnostic, when compared to the OSE diagnostic, is also shown for the 00 UTC analysis cycles.

3.1. Contribution of the observations to forecast error

3.1.1. Summer

The impact of the operational data set on the 24 hour forecast error has been investigated from the 15 June to 15 July 2006 at 00 and 12 UTC (summer 2006). The forecast error for which the FSO is based is computed from the *control* experiment of the OSEs (see Table 1 and Table 2). The global observation performance over this month, as described in 2.11, is summarized in Fig.1. Negative (positive) values correspond to a decrease (increase) of forecast error due to a specific observation type.

The largest error decrease is due to AMSU-A (four satellites) and AIRS radiances followed by SYNOP (mainly surface pressure), AIREP and DRIBU (mainly surface pressure) conventional observations. Good error reduction is also observed from SCAT (Quikscat and ERS scatterometer) and AMSU-B radiance observations. An increase of forecast error is caused by AMVs (Atmospheric Motion Vector) from geostationary satellites. Some degradation is also observed from PILOT observations.

A more detailed diagnostic of the forecast error contribution from AMVs is shown in Fig.2. The contribution to the forecast error of the observed u-wind component is grouped by pressure levels, satellite types, such as GOES (G, two geostationary satellites GOES-8 and 9), METEOSAT (M, two geostationary satellites METEOSAT-7 and 8) and MODIS polar instruments (MO, MODIS Terra and Aqua), and by frequency bands: infrared (IR), visible (V) and water vapour (WV). The largest degradation is due to the visible and infrared frequency band at levels below 700 hPa, (mainly at 850 hPa) from METEOSAT (to a larger extent) and from the GOES satellites.

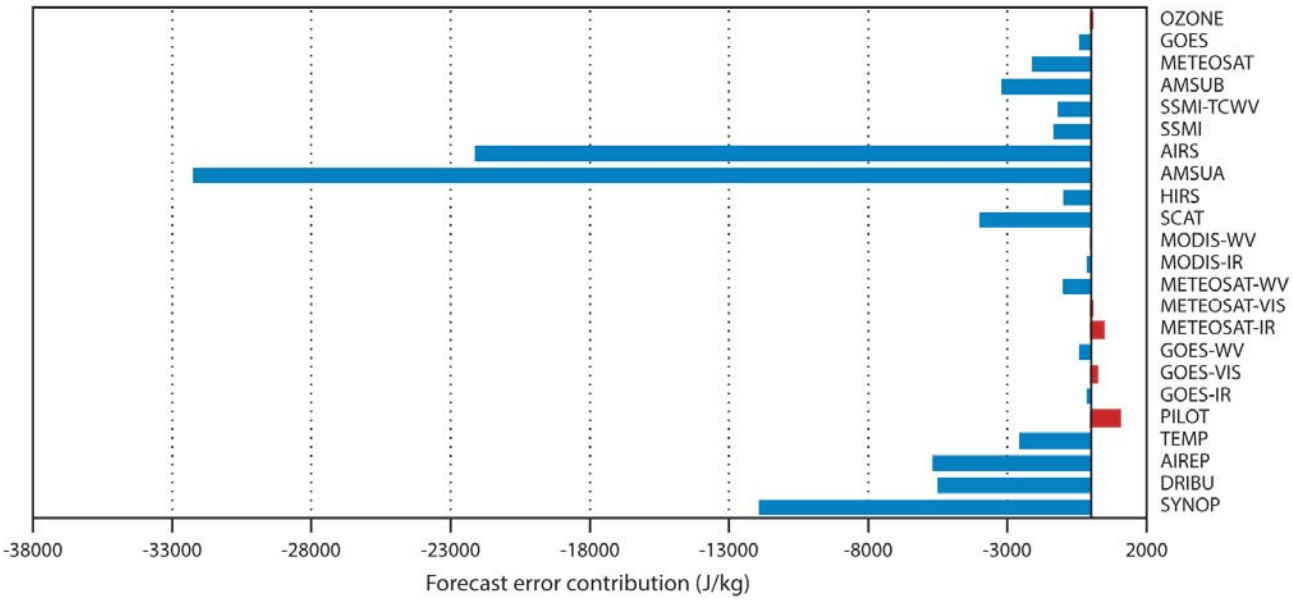

Figure 1: 24-hour forecast error contribution in J/kg of the components (types) of the observing system in summer 2006. Negative (positive) values correspond to a decrease (increase) in the energy norm of forecast error.

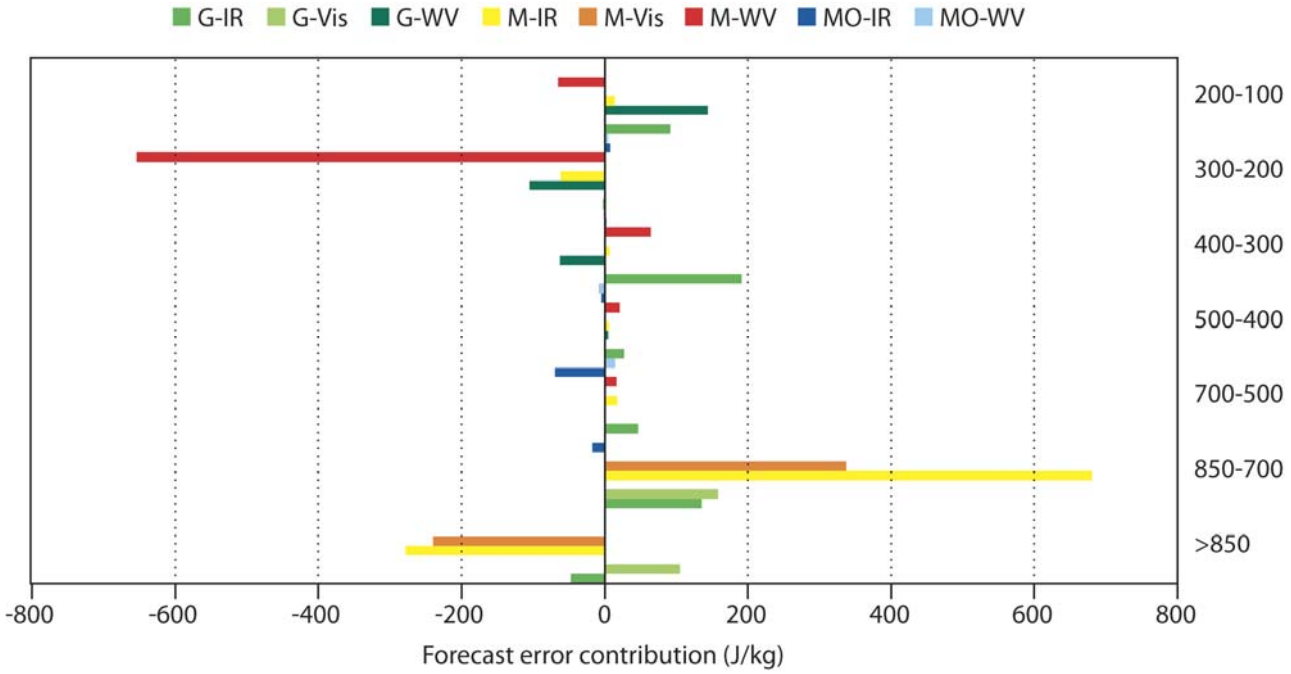

Figure 2: Forecast error contribution of the observed u-component of the wind on pressure levels and grouped by satellite types: GOES (G, two satellites GOES-8 and 9), METEOSAT (M, two satellite METEOSAT-7 and 8) and MODIS (MO, two satellites: Terra and Aqua) and by frequency bands: infrared (IR), visible (V) and water vapour (WV). Negative (positive) values correspond to a decrease (increase) of forecast error

The geographical locations of the degradation are shown in Fig 3 which displays the 00 UTC forecast error contribution of the visible and infrared bands between 1000 and 700 hPa accumulated over the summer month. The largest degradation is found over the southern equatorial band, in particular over the Atlantic (area-1) and Indian ocean (area-2) where the METEOSAT satellites are located, followed by the one over the West Pacific (area-3) where GOES operates.

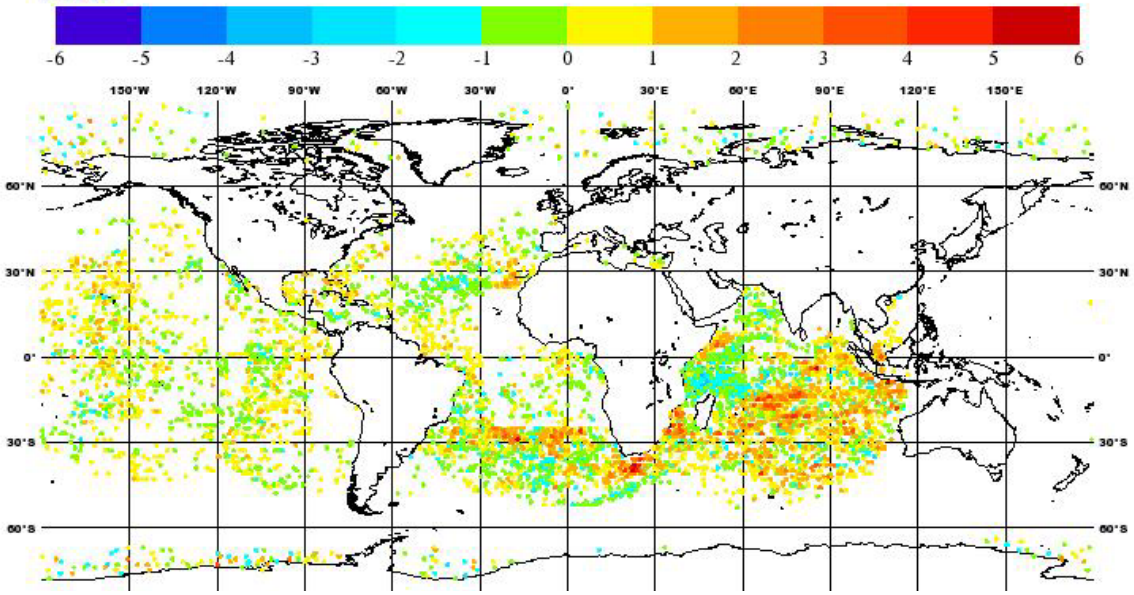

Figure 3: 00 UTC forecast error contribution (J/kg) of the observed u-component of the wind between 700 and 1000 hPa from GOES and METEOSAT visible wavelength bands accumulated over one month in summer 2006. Negative (positive) values correspond to a decrease (increase) of forecast error.

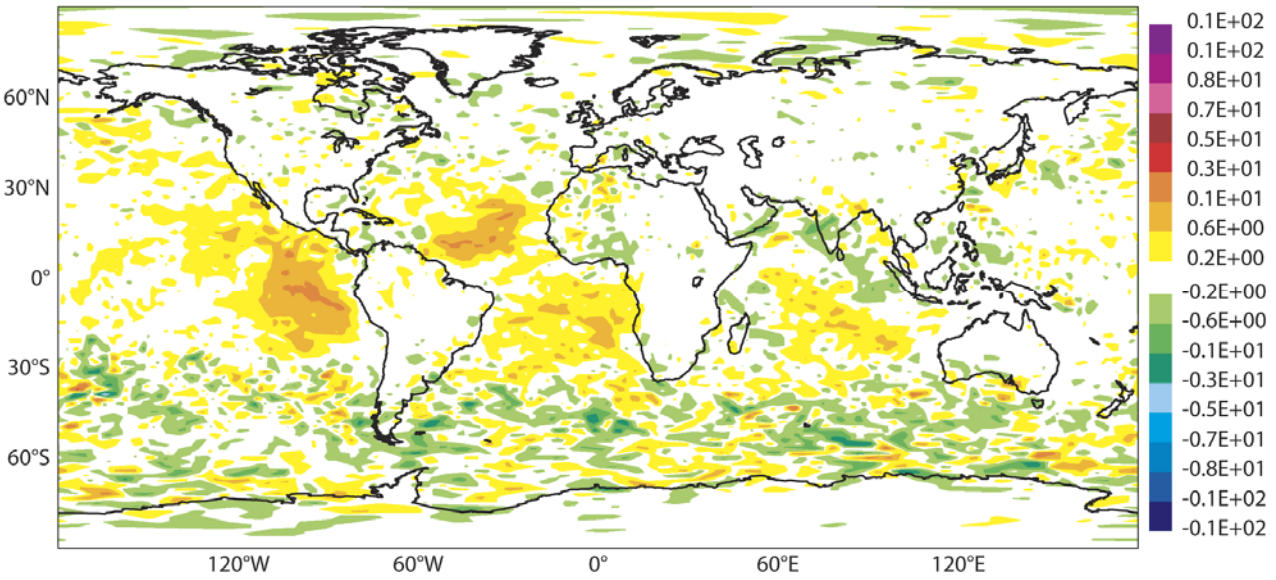

Figure 4: rms forecast error differences between AMV and Reference OSEs of the 24 hour forecast starting at 00UTC for the u-component of the wind at 850 hpa (m/s). Positive (negative) contours indicate AMV errors are larger (smaller) than Reference errors.

The impact of AMVs on the forecast has also been assessed through the OSE. Among the different OSEs performed at ECMWF, one in particular was performed to measure the impact of assimilated AMVs by comparing the *reference* experiment (all conventional observations plus AMSU-A radiances from NOAA-16) with an experiment containing AMV observations in addition to the observations used in *reference* (see Table 2). Figure 4 shows the *rms* (root mean square) forecast error differences between Reference and AMV experiments for the 24-hour forecast starting at 00 UTC for the 850 hPa u-wind component. Similar degradation appears in area-1, area-2 and area-3 defined above The largest degradation in the South Pacific (Fig. 4) is supported to a lesser extent by FSO diagnostic (Fig. 3).

In the Indian Ocean, a well established Indian Monsoon circulation was taking place, characterized by a strong low level wind from South-East towards the Indian continent (fig. 5). Such situation is not well represented by the model that tends to reinforce too much the low level circulation. The degradation due to the AMV in the area-2 is therefore likely attributed to a model bias. On the contrary, over the South of the Atlantic ocean (area-1) due to the presence of semi-permanent anti-cyclone circulation in the tropical band, the associated large scale subsidence (Fig.6) reinforces the trade inversion with a subsequent suppression of deep clouds (around 30 degrees), leaving only the shallow ones. Figure 6 shows a cross section (35W, 0E) of the average vertical velocity for the same period, indicating the large cell of subsidence at 30S. This synoptic situation has implication with the methodology applied by the data provider to measure the height of the top of the clouds, resulting in a degradation of the data quality. A modified analysis experiment by reassigning the height of the top of the clouds according to the model first guess instead of using the height assigned by the data provider (courtesy of Niels Bormann) was performed to address the point. Unfortunately, the FSO based on the new forecast error does not indicate a significant improvement. The causes of the degradations are still under investigation. Similar synoptic situation to area-2 is also noticed in area-3, it is therefore believed that, even for this case, the degradation is attributed to the data quality.

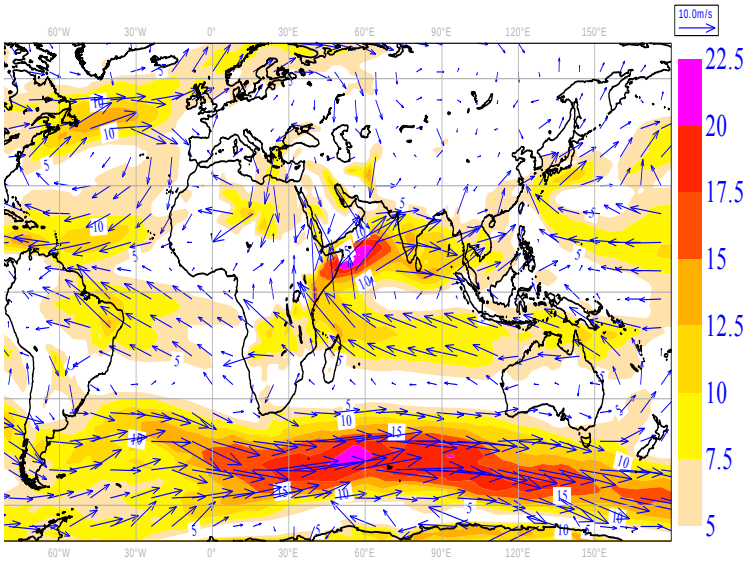

Figure 5: 850 hPa mean wind field over the Summer period. Shading contours indicate the wind speed.

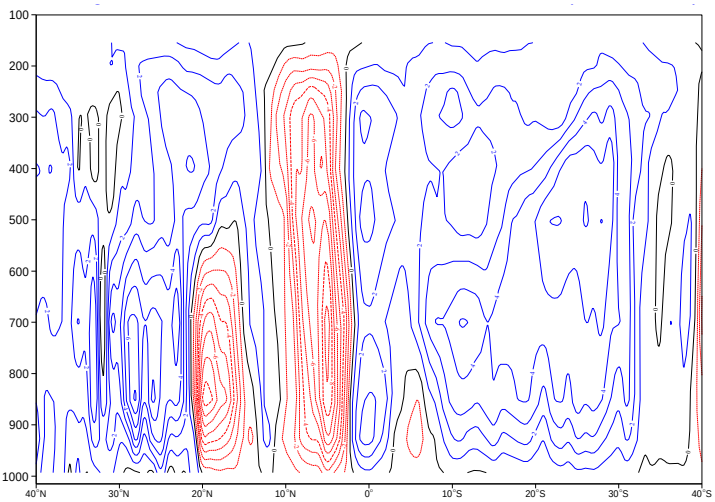

Figure 6: Mean vertical velocity over the Summer period. The strong sinking motion in Southern Hemisphere near 30S represents the limit of the Hadley circulation characterized by the subtropical high pressure cell.

Figure 1 shows also a forecast error increase due to PILOT observations (Table 1). The geographical display of the forecast error for PILOT observations (not shown) indicates that the degradation was coming from the American wind profilers. Problems with the American wind profilers at low levels (below 700 hPa) were known in spring time due to bird migration contamination (Wilczak *et al*. 1995). But other meteorological situations also produce a contamination of profiler measurements (Ackley *et al*. 1998), one of which is the limitation of the local horizontal atmospheric uniformity assumption that must be satisfied to have a correct mean wind measure. Meteorological conditions in which short spatial and temporal scales of variability have amplitudes as large as the mean, as for example in the presence of a CBL (Convective Boundary Layer) and severe storms, limit the horizontal wind measurement. It was effectively found that the CBL-activity was rather high for this period as can be see from the large height of the boundary layer at the station locations, averaged among all profiler stations (Fig. 7).

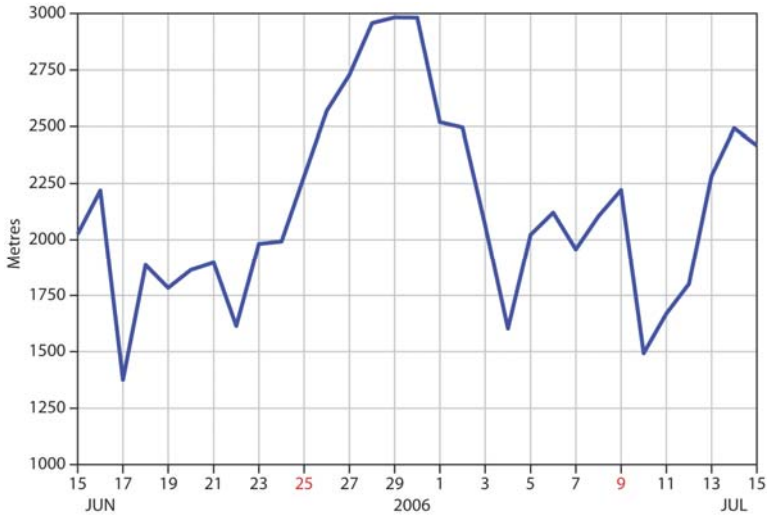

Figure 7: Time series of averaged boundary layer top height from 21-hour forecasts valid at 15:00 local time of all American wind profile stations over the summer period.

It was also found that both CAPE and TCWV compared with the ERA climatology (Uppala *et al*. 2005) indicated larger CAPE and humidity advection from the Golf of Mexico in areas where wind profilers are located (not shown). Together, high TCWV and CAPE, triggered the convection activity. The lessons learnt with wind profilers is that their impact on the forecast can change quite a lot given the meteorological situations, therefore monitoring their impact on forecast skill, on a daily basis, would allow a more efficient screening of the contaminated measurements.

3.1.2. Winter

The winter period examined in this paper ranges from the 5 of January to the 12 of February 2007. On the 24-hour forecast error the global observation performance (Fig.8) is very similar to the summer performance (Fig. 1). Some forecast skill deteriorations are again produced by METEOSAT and GOES AMVs obtained from the visible and infrared band

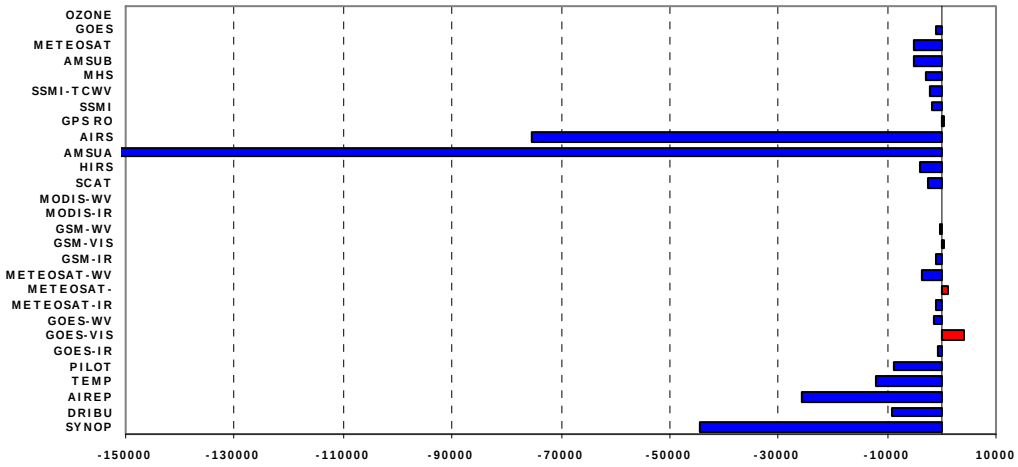

Figure 8: 24-hour forecast error contribution in J/kg of the components (types) of the observing system in winter 2007. Negative (positive) values correspond to a decrease (increase) in the energy norm of forecast error.

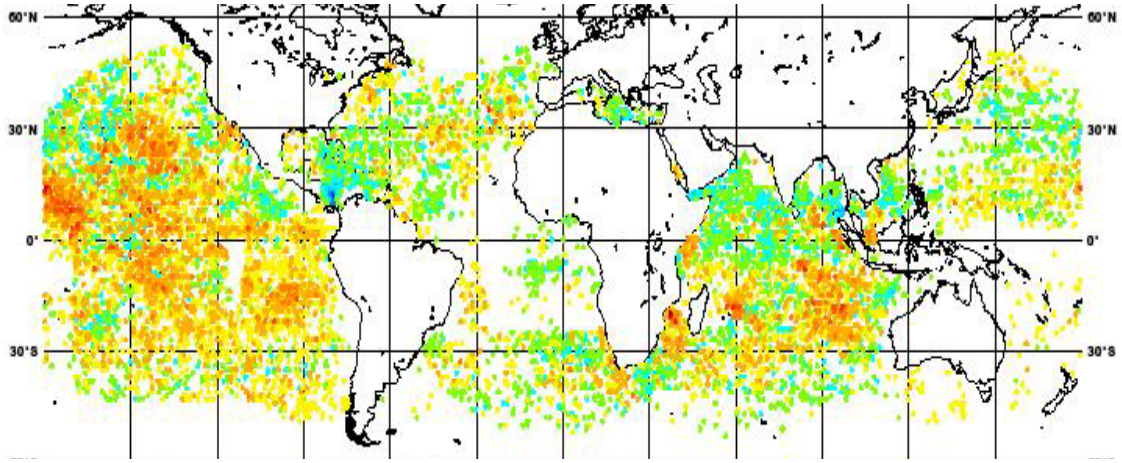

Figure 9: 00 UTC forecast error contribution (J/kg) of the observed u-component of the wind between 700 and 1000 hPa from GOES and METEOSAT visible wavelength bands accumulated over one month in winter 2007. Negative (positive) values correspond to a decrease (increase) of forecast error.

A large degradation is observed in central eastern Pacific ocean where a large convective activity is taking place due to El Nino condition (not shown). The largest negative impact of AMVs to the Fc error is found (Fig. 9) between 5N and 15N and coincides with a broad downward mean motion of the Hadley circulation (large departures were found below 700-hPa in the same region, not shown). The second cluster of negative impact near 25N-140W is localized on top of a region of weak winds with strong sinking motion in a high pressure system. Both synoptic situations are critical for the measuring the height of the top of the clouds, consequently the degradation is associated with the quality of the data.

In general, the impact on the forecast of the observations can be negative for different reasons that can be related to the data quality or other weaknesses of the assimilation system. It has been found that biases in the model can deteriorate the assimilation of good sources of information.

4. Conclusions

Over the last few years, the potential of using derived adjoint-based diagnostic tools has been increasingly exploited. This paper illustrates the use of the forecast sensitivity with respect to time-distributed observational data, first time in a 12-hour 4D-Var assimilation system, as a diagnostic tool to monitor the observation performance in the short-range forecast.

Here, the forecast sensitivity to the observation has been based on the forecast error of the *control* experiment from observing system experiments that have been performed at ECMWF, with the intention of comparing the performance of the two diagnostic tools. The assessment of the value of observations for forecast error reduction trough the OSEs is performed by comparing the forecast skill obtained with and without the subset of data of interest. This usually involves large numbers of independent experiments over several months and is therefore quite expensive to perform and prohibitive if a detailed investigation of operational observing systems must be obtained. Also, any variation in the observation set that is assimilated through data addition or data denial modifies the Kalman gain matrix, producing therefore different solutions in the minimization. However, observation forecast impact on the medium and long-range can also be investigated. On the short-range forecast, FSO and OSE provide a very similar qualitative picture of forecast

improvement or degradation. In conclusion, OSEs are more indicated for evaluating the longer term forecast impact of data whilst FSO should be used to investigate the reasons of short-range forecast failure.

Forecast sensitivity to observations can only be used to diagnose the impact on the short-range forecast, namely 24 to 48 hours, given the use of a simplified adjoint of the data assimilation system and the implied linearity assumption. FSO allows the identification of potential problems and directs further investigations through the further granularity on observation type, level and channel at no extra cost.

Over the two months period, the global impact of observations was found to be positive and the forecast errors decrease for almost all data type. Problems have been noticed with Atmospheric Motion Vectors mainly derived from visible and infrared wavelength bands (and for low-level winds). Some of the problems were associated with the data quality and others to the model bias. Also, in summer, the wind profiler measurements were corrupted by the presence of strong convection activity in the boundary layer. Given the dependency of some observation types on the meteorological situation, it is suggested to run the forecast sensitivity to the observation diagnostic tool on an operational basis and in relation to the operational suite error. A constant monitoring of the performance of the model forecast would allow the use of the observation network in an adaptive way where situation with negative observation impact can be investigated and improved or potentially denied in real time.

5. References

Ackley M., R. Chadwick J. Cogan, C. Crosiar, F. Eaton, K.Gage, E. Gossard, R. Lucci, F. Merceret, W. Neff, M. Ralph, R. Strauch, D. Van de Kamp, B. Weber, A. White, 1998: U.S. Wind Profilers: A review. FCM-R14-1998

Baker N.L. and R. Daley, 2000: Observation and background adjoint sensitivity in the adaptive observation targeting problem. *Q. J. R. Meteorol. Soc*, **126**,1431-1454

Bouttier, F, and Kelly, G., 2001: Observing system experiments in the ECMWF 4D-Var data assimilation system. *Q. J. R. Meteorol. Soc*, **127**,1469-1488

Cardinali, C., S. Pezzulli and E. Andersson, 2004: Influence matrix dagnostics of a data assimilation system. *Q. J. R. Meteorol. Soc.*, **130,** 2767—2786

Cardinali, C., and R. Buizza: 2004. Observation sensitivity to the analysis and the forecast: a case study during ATreC targeting campaign. Proceedings of the First THORPEX International Science Symposium, 6-10 December 2004, Montreal, Canada, WMO TD 1237 WWRP/THORPEX N. 6.

Chapnik, B., G.Desnrozier, F. Rabier and O. Talagrand, 2006: Diagnosis and tuning of observation error in a quasi-operational data assimilation setting. *Q. J. R. Meteorol. Soc.*, **132,** 543—565.

Courtier P., E. Andersson, W. Heckley, J. Pailleux, D. Vasiljevic, M. Hamrud, A. Hollingsworth, F. Rabier and M. Fisher, 1998: The ECMWF implementation of three-dimension variational assimilation (3D-Var). Part I: Formulation. *Q. J. R. Meteorol. Soc.*, **124,** 1783—1807

Daescu, D.N., 2008: On the sensitivity equations of 4D-Var data assimilation. *Mon. Wea. Rev.*, accepted for publication.

English, S., R. Saunders, B. Candy, M. Forsythe, and A. Collard, 2004: Met Office satellite data OSEs. Third WMO Workshop on the impact of various observing systems on numerical weather prediction, Alpbach, Austria, WMO/TD, **1228**, 146-156

Errico, R., 2007: Interpretation of an adjoint-derived observational impact measure. *Tellus*, **59A**, 273-276.

Fisher, M., 2003: Estimation of entropy reduction and degrees of freedom for signal for large variational analysis systems. *ECMWF Tech. Memo.*, **397,** pp 18.

Gelaro R, Buizza, R., Palmer T.N. and Klinker E., 1998: Sensitivity analysis of forecast errors and the construction of optimal perturbations using singular vectors. *J. Atmos. Sci.*, **55**, 1012—1037.

Kelly, G., and Thépaut, J-N 2007: Evaluation of the impact of the space component of the Global Observation System through Observing System Experiments. ECMWF Newsletter No 113, 16-28.

Isaksen L., M. Fisher, E. Andersson, and J. Barkmeijer 2005: The structure and realism of sensitivity perturbations and their interpretation as 'Key Analysis'. *Q. J. R. Meteorol. Soc*, **131**, 3053—3078.

Langland R. and N.L Baker., 2004: Estimation of observation impact using the NRL atmospheric variational data assimilation adjoint system. *Tellus,* **56A,** 189-201.

Lorenc, A., 1986: Analysis methods for numerical weather prediction. *Q. J. R. Meteorol. Soc.*, **112,** 1177—1194.

Lopez, P. and E. Moreau, 2005: A convection scheme for data assimilation: Description and initial tests. *Q.J.R.Meteorol.Soc*., **131**, 409—436

Lord, S., T. Zapotocny, and J. Jung, 2004: Observing system experiments with NCEP's global forecast system.Third WMO Workshop on the impact of various observing systems on numerical weather prediction, Alpbach, Austria, WMO/TD, **1228**, 56-62.

Janiskova, M., J.-J. M. J.-F. Mahfouf, and F. Chevallier, 2002: Linearized radiation and cloud schemes in the ECMWF model: Development and evaluation, *Q. J. R. Meteorol. Soc*., **128**, 1505—1527.

Purser, R. J. and Huang, H.-L.,1993: Estimating Effective Data Density in a Satellite Retrieval or an Objective Analysis. *J. Appl. Meteorol.*, **32,** 1092—1107.

Rabier, F. and Courtier, P., 1992: Four-dimensional assimilation in the presence of baroclinic instability. *Q. J. R. Meteorol. Soc.*, **118,** 649—672.

Rabier, F., Klinker, E., Courtier, P. and Hollingsworth A. 1996: Sensitivity of forecast errors to initial condition. *Q. J. R. Meteorol. Soc*. **122**, 121—150

Rabier, F., Järvinen, H., Klinker, E., Mahfouf J.F., and Simmons, A., 2000: The ECMWF operational implementation of four-dimensional variational assimilation. Part I: experimental results with simplified physics. *Q. J. R. Meteorol. Soc*. **126,** 1143—1170.

Talagrand, O., 1997: Assimilation of observations, an Introduction. *J. Meteorol. Soc. Japan*, **Vol 75,** N.1B,191—209.

Talagrand O., 2002: A posteriori validation of assimilation algorithms. Proceding of NATO Advanced Study Institute on Data Assimilation for the Earth System, Acquafreda, Maratea, Italy.

Tompkins, A.M. and M. Janiskova: 2004, A cloud scheme for data assimilation: Description and initial tests. *Q.J.R.Meteorol.Soc*,**130**, 2495—2517

Uppala, S.M., Kållberg, P.W., Simmons, A.J., Andrae, U., da Costa Bechtold, V., Fiorino, M., Gibson, J.K., Haseler, J., Hernandez, A., Kelly, G.A., Li, X., Onogi, K., Saarinen, S., Sokka, N., Allan, R.P., Andersson, E., Arpe, K., Balmaseda, M.A., Beljaars, A.C.M., van de Berg, L., Bidlot, J., Bormann, N., Caires, S., Chevallier, F., Dethof, A., Dragosavac, M., Fisher, M., Fuentes, M., Hagemann, S., Hólm, E., Hoskins, B.J., Isaksen, L., Janssen, P.A.E.M., Jenne, R., McNally, A.P., Mahfouf, J.-F., Morcrette, J.-J., Rayner, N.A., Saunders, R.W., Simon, P., Sterl, A., Trenberth, K.E., Untch, A., Vasiljevic, D., Viterbo, P., and Woollen, J. 2005: The ERA-40 re-analysis. *Q. J. R. Meteorol. Soc.*, **131**, 2961—3012.

Van der Vorst, H.A., 2003: Iterative Krylov methods for large linear systems. *Cambridge Accademic Press*

Wilczak, J., R. Strauch, F. Ralph, B. Weber, D. Merritt, J. Jordan, D. Wolfe, L. Lewis, D. Wuertz, J. Gaynor, S. McLaughlin, R. Rogers, A. Riddle, and T. Dye, 1995: Contamination of Wind Profiler Data by Migrating Birds: Characteristics of Corrupted Data and Potential Solutions. *J. Atmos. Oceanic Technol*., **12**, 449-467.

Zhu, Y. and Gelaro, R., 2008: Observation Sensitivity Calculations Using the Adjoint of the Gridpoint Statistical Interpolation (GSI) Analysis System. *Mon. Wea. Rev.*, **136,** 335—351.